Molecular beam epitaxy of $Co_xFe_{4-x}N$ ($0.4<x<2.9$) thin films on $SrTiO_3$(001) substrates

Tatsunori Sanai, Keita Ito, Kaoru Toko, Takashi Suemasu

Institute of Applied Physics, Graduate School of Pure and Applied Sciences, University of Tsukuba, 1-1-1 Tennohdai, Tsukuba, Ibaraki 305-8573, Japan

Abstract

We attempted to grow $Co_xFe_{4-x}N$ epitaxial thin films on $SrTiO_3$(001) substrates by molecular beam epitaxy supplying solid Co and Fe and a radio frequency N_2 plasma, simultaneously. The composition ratio of Co/Fe in $Co_xFe_{4-x}N$ was controlled by changing the weight ratio of Co to Fe flakes in the crucible of the Knudsen cell used. We confirmed epitaxial growth of $Co_xFe_{4-x}N$ ($0.4<x<2.9$) thin films by reflection high-energy electron diffraction and θ-2θ X-ray diffraction patterns. The in-plane lattice parameter of the $Co_xFe_{4-x}N$ films was almost the same as the out-of-plane lattice parameter, and they decreased with increasing Co composition, following Vegard's law.

Keywords: A3.Molecular beam epitaxy, B2.Ferromagnetic materials, B1.$Co_xFe_{4-x}N$, B1.$SrTiO_3$

1. Introduction

Highly spin-polarized ferromagnetic materials have attracted increasing attention for high-performance spintronics devices such as the read heads of hard disc drives and spin random access memory. For these materials, special attention has been focused on cubic perovskite 3*d* ferromagnetic nitrides such as Fe_4N and Co_4N. The spin asymmetry $\beta = (\sigma_\uparrow - \sigma_\downarrow)/(\sigma_\uparrow + \sigma_\downarrow)$ of Fe_4N was calculated to be −1.0 [1], and we evaluated $|\beta|$ to be 0.59 at 7.8 K by means of point contact Andreev reflection measurement [2]. There have been a few reports on the inverse tunnel magnetoresistance of −75% in CoFeB/MgO/Fe_4N magnetic tunnel junctions and negative anisotropic magnetoresistance in Fe_4N films at room temperature [3-6]. The spin-resolved density of states (*D*) in Co_4N was calculated [7,8], and spin polarization $P = (D_\uparrow - D_\downarrow)/(D_\uparrow + D_\downarrow)$ at the Fermi level was estimated to be −0.88 by Imai *et al*., which exceeds that in Fe_4N of −0.67 [8]. We have already succeeded in epitaxial growth of Fe_4N and Co_4N thin films on $SrTiO_3$(STO)(001) substrates by molecular beam epitaxy (MBE) [9,10] and we evaluated the spin and orbital magnetic moments by X-ray magnetic circular dichroism [11,12]. Recent first-principles calculation indicating that *P* was estimated to be −1.0 in Co_3FeN has renewed interest in this material [13]. There have been several reports on perovskite mixed crystal nitrides such as $(Co,Fe)_4N$ and $(Mn,Fe)_4N$. H. Y. Wang *et al*. formed CoFeN films by radio frequency (RF) magnetron sputtering and evaluated their magnetic anisotropy [14-16]. First-principles calculations were performed for the electronic and

magnetic structures in $(Mn,Fe)_4N$ [17-20]. D. L. Peng *et al*. characterized perpendicular magnetic anisotropy of $(Fe,Cr)_4N_x$ films formed by DC magnetron sputtering [21-23]. However, there have been no reports so far on epitaxial growth of $(Co,Fe)_4N$ thin films. In order to apply $(Co,Fe)_4N$ films to spintronics devices, characterization of the basic material properties of high quality $(Co,Fe)_4N$ films is required. In this study, we attempted to grow $(Co,Fe)_4N$ epitaxial films on STO(001) substrates by MBE, while varying the composition ratio of Co/Fe in $(Co,Fe)_4N$.

2. Experimental procedures

Approximately 25-nm-thick $(Co,Fe)_4N$ thin films were grown on STO(001) substrates by supplying Co, Fe and N atoms simultaneously using an ion-pumped MBE system equipped with a high-temperature Knudsen cell for Co and Fe, and an RF-N_2 plasma for N [9,10]. The lattice mismatch between Fe_4N and STO is 2.8%, and that between Co_4N and STO is 4.3%. Co and Fe flakes were placed into the same crucible. Various weight ratios of Co/Fe in the crucible were used including 0.5:1 (sample A), 1:1 (sample B), 3:1 (sample C) and 5.6:1 (sample D). During the growth of these samples, the temperature of the STO substrate was kept at 450 ºC, and the deposition rate of Co plus Fe was set to be approximately 0.5 nm/min. The flow rate of the N_2 gas was fixed at 1.0 sccm, and the input power to the RF plasma was 140 W. The pressure inside the chamber was approximately 1×10^{-4} Torr during film growth.

58 The crystalline quality of samples A-D was evaluated by reflection high-energy electron
59 diffraction (RHEED) and θ-2θ X-ray diffraction (XRD). We deduced the lattice constants of
60 samples along directions perpendicular and parallel to the substrate surface from out-of-plane
61 and in-plane θ-2θ XRD patterns, respectively. The composition ratio of Co/Fe in the films
62 was determined by energy dispersive X-ray spectroscopy (EDX) using an accelerating voltage
63 of 10 kV with a spot size of 30 μm and by Rutherford back scattering spectrometry (RBS)
64 using a He ion beam with an acceleration voltage of 2.3 MeV.
65
66 **3. Results and discussion**
67 Figures 1(a)-1(d) show the RHEED patterns of samples A-D, respectively. Streaky
68 RHEED patterns were obtained except for the spotty pattern for sample B. Figure 2(a) shows
69 the out-of-plane θ-2θ XRD patterns of Fe_4N/STO(001), and Figs. 2(b)-2(e) show those of
70 samples A-D, respectively. In samples A-D, the diffraction peaks of $(Co,Fe)_4N$(001), (002)
71 and (004) were observed. With increasing weight ratio of Co to Fe in the crucible, these
72 peaks shifted to a higher angle. Figures 3(a)-3(d) show the in-plane θ-2θ XRD patterns of
73 samples A-D around 2θ=23°, respectively. The diffraction peaks of $(Co,Fe)_4N$(100) were
74 clearly observed in these samples. With increasing weight ratio of Co to Fe in the crucible,
75 these peaks also shifted to a higher angle. According to the X-ray extinction law, the
76 diffraction peak of fcc-Co(100) is forbidden; however, that of $(Co,Fe)_4N$(100) is allowed.

The experimentally obtained intensity ratios of (100) to (200) were 0.0096, 0.0092, 0.0074, and 0.0079, in samples A-D, respectively. In the case of Co_4N, the intensity ratio is theoretically estimated to be 0.027. Therefore, we can state that the grown layers are not fcc-Co, but $(Co,Fe)_4N$ in which N atom is located at the body center of the unit cell. On the basis of these results, we confirmed that the $(Co,Fe)_4N$ layers grew epitaxially on the STO(001) substrates. At present, we cannot determine the degree of order of N atoms. It can be estimated, for example, by comparing the experimentally obtained intensity ratios of (100) to (200) with theoretical ones. However, information about Fe and Co sites in the unit cell of $(Co,Fe)_4N$ is limited at present, and thus further studies are mandatory for this estimation. A small diffraction peak of Fe(002) in Figs. 2(b)-2(e) indicate that pure Fe exists in the $(Co,Fe)_4N$ layers of samples A-D. However, the peak intensities were negligibly small compared to those of $(Co,Fe)_4N$. Thus, we consider that the analysis of the composition ratio Co/Fe in the $(Co,Fe)_4N$ layers of samples A-D was not affected by the existence of pure Fe, if there was any present. In order to determine the Co/Fe composition ratio in the $(Co,Fe)_4N$ layers using EDX measurements, we grew an Au(5 nm)/$(Co,Fe)_4N$(12 nm) film on the MgO(001) substrate (sample E) using the same growth procedure as sample C, and evaluated the composition ratio of Co, Fe and N using RBS measurements.

Figure 4 shows the RBS depth profiles of Co, Fe, N, Au, Mg and O atoms in sample E. The composition ratio in the $(Co,Fe)_4N$ layer was evaluated to be approximately Co:Fe =

96 1.4:1.0, and (Co+Fe):N = 4:1. We assumed that the composition ratio of $(Co,Fe)_4N$ in sample
97 C was the same as that in sample E, and we estimated the Co/Fe ratio in sample C to be
98 $Co_{2.3}Fe_{1.7}N$. Figures 5(a)-5(d) show the EDX spectra of samples A-D, respectively. Peaks of
99 Co K_α (6.924 keV) and Fe K_β (7.057 keV) X-rays partially overlapped. We separated the
100 overlapped peak into two peaks using Gaussian curve fitting. The integrated intensity of the
101 Co K_α X-ray peak was enhanced with increasing weight ratio of Co/Fe in the crucible. On
102 the other hand, the integrated intensity of the Fe K_α X-ray peak was relatively suppressed.
103 We determined the composition ratio in the $(Co,Fe)_4N$ layers of samples A, B and D using
104 the RBS measurements for sample E and obtained EDX spectra of samples A-D. First, we
105 deduced a constant value γ using

106 $$\frac{EDX_{CoK\alpha}}{EDX_{FeK\alpha}} = \gamma \frac{RBS_{Co}}{RBS_{Fe}}, \qquad (1)$$

107 where $EDX_{CoK\alpha} / EDX_{FeK\alpha}$ is the ratio of integrated EDX intensity of Co K_α to Fe K_α
108 X-rays in sample C, and RBS_{Co} / RBS_{Fe} is the composition ratio of Co/Fe in sample E
109 obtained by the RBS depth profiles shown in Fig. 4. We evaluated the composition ratio of
110 Co/Fe in $(Co,Fe)_4N$ layers for samples A, B and D using $EDX_{CoK\alpha} / EDX_{FeK\alpha}$ of these
111 samples divided by the constant γ to be $Co_{0.4}Fe_{3.6}N$, $Co_{1.2}Fe_{2.8}N$ and $Co_{2.9}Fe_{1.1}N$, respectively,
112 as summarized in Table 1.

113 Figure 6(a) shows the out-of-plan lattice constants of samples A-D deduced from
114 $(Co,Fe)_4N(002)$ and $(Co,Fe)_4N(004)$ θ-2θ XRD peak positions plotted as a function of $\cot\theta$.

The peak positions were determined by Gaussian fitting for the XRD patterns, and lattice constants were deduced by Bragg's law. Figure 6(b) shows the out-of-plane lattice constants of samples A-D after correction of the measurement error, by extrapolating from the intersection of the straight line passing through the above two points at $\cot\theta = 0$ in Fig. 5(a), plotted against the composition ratio of $Co_xFe_{4-x}N$. A dashed line is drawn for Vegard's law [24] using the bulk lattice constants of Fe_4N (0.3796 nm) [25] and Co_4N (0.3738 nm) [26]. The out-of-plane lattice constants of samples A-D were 0.3793, 0.3768, 0.3761 and 0.3750 nm, respectively. Figures 7(a)-7(b) show the case of in-plane θ-2θ XRD measurements. In-plane lattice constants for samples A-D were deduced to be 0.3788, 0.3775, 0.3755 and 0.3737 nm, respectively, using the same method as the out-of-plane case. Both out-of-plane and in-plane lattice constants decreased with increasing Co/Fe ratio in $Co_xFe_{4-x}N$, and they followed Vegard's law. There was no significant difference between out-of-plane and in-plane lattice constants, indicating that the lattice was almost strain-free.

4. Conclusions

We have succeeded in growing $Co_xFe_{4-x}N$ ($0.4<x<2.9$) thin films epitaxially on STO(001) substrates by MBE supplying solid Co, Fe, and RF-N_2, simultaneously. We were able to control the composition ratio of Co/Fe in $(Co,Fe)_4N$ by changing the weight ratio of Co to Fe flakes in the crucible. The lattice constants of the grown films decreased with

increasing Co/Fe ratio, and they were in good agreement with Vegard's law. We also confirmed that the lattice was almost relaxed in the 25-nm-thick $(Co,Fe)_4N$ films on STO(001).

Acknowledgements

In-plane XRD measurements were performed with the help of Dr. Y. K. Takahashi, Dr. T. Furubayashi and Prof. K. Hono of the National Institute for Materials Science (NIMS), Tsukuba and the Rigaku Corporation. The authors thank Dr. Y. Imai of the National Institute of Advanced Industrial Science and Technology (AIST), Tsukuba, for useful discussions.

References

[1] S. Kokado, N. Fujima, K. Harigaya, H. Shimuzu, A. Sakuma, Phys. Rev. B **73** (2006) 172410.

[2] A. Narahara, K. Ito, T. Suemasu, Y. K. Takahashi, A. Rajanikanth, K. Hono, Appl. Phys. Lett. **94** (2009) 202502.

[3] Y. Komasaki, M. Tsunoda, S. Isogami, M. Takahashi, J. Appl. Phys. **105** (2009) 07C928.

[4] M. Tsunoda, Y. Komasaki, S. Kokado, S. Isogami, C. C. Chen, M. Takahashi, Appl. Phys. Express **2** (2009) 083001.

[5] M. Tsunoda, H. Takahashi, S. Kokado, Y. Komasaki, A. Sakuma, M. Takahashi, Appl. Phys. Express **3** (2010) 113003.

[6] K. Ito, K. Kabara, H. Takahashi, T. Sanai, K. Toko, T. Suemasu, M. Tsunoda, Jpn. J. Appl. Phys. **51** (2012) 068001.

[7] S. F. Mater, A. Houari, M. A. Belkhir, Phys. Rev. B **75** (2007) 245109.

[8] Y. Imai, Y. Takahashi, T. Kumagai, J. Magn. Magn. Mater. **322** (2010) 2665.

[9] K. Ito, G. H. Lee, H. Akinaga, T. Suemasu, J. Cryst. Growth **322** (2011) 63.

[10] K. Ito, K. Harada, K. Toko, H. Akinaga, T. Suemasu, J. Cryst. Growth **336** (2011) 40.

[11] K. Ito, G. H. Lee, K. Harada, M. Suzuno, T. Suemasu, Y. Takeda, Y. Saitoh, M. Ye, A. Kimura, H. Akinaga, Appl. Phys. Lett. **98** (2011) 102507.

[12] K. Ito, K. Harada, K. Toko, M. Ye, A. Kimura, Y. Takeda, Y. Saitoh, H. Akinaga, T.

163 Suemasu, Appl. Phys. Lett. **99** (2011) 252501.

164 [13] Y. Takahashi, Y. Imai, T. Kumagai, J. Magn. Magn. Mater. **322** (2011) 2941.

165 [14] H. Y. Wang, E. Y. Jiang, Z. W. Ma, Y. J. He, H. S. Huang, J. Phys. Condens. Matter. **11**

166 (1999) 989.

167 [15] K. K. Shih, J. Karasinski, J. Appl. Phys. **73** (1993) 8377.

168 [16] N. D. Ha, B. C. Parka, H. B. Kima, C. G. Kima, C. O. Kim, J. Magn. Magn. Mater. **286**

169 (2005) 267.

170 [17] C. A. Kuhnen, A. V. dos Santos, J. Magn. Magn. Mater. **130** (1994) 353.

171 [18] C. Paduani, J. Appl. Phys. **96** (2004) 1503.

172 [19] M. S. Patwari, R. H. Victora, Phys. Rev. B **64** (2001) 214417.

173 [20] L. Chen, J. Appl. Phys. **100** (2006) 113717.

174 [21] D. L. Peng, K. Sumiyama, T. J. Konno, K. Suzuki, Jpn. J. Appl. Phys. **36** (1997) L479.

175 [22] D. L. Peng, T. J. Konno, K. Sumiyama, H. Onodera, K. Suzuki, J. Magn. Magn. Mater.

176 **172** (1997) 41.

177 [23] D. L. Peng, K. Sumiyama, K. Suzuki, J. Alloys Compd. **265** (1998) 49.

178 [24] L. Vegard, Z. Phys. **5** (1921) 17.

179 [25] H. Jacobs, D. Rechenbach, U. Zachwieja, J. Alloys Compd. **227** (1995) 10.

180 [26] N. Terao, Mem. Sci. Rev. Met. **57** (1960) 96.

181

Figs. 1. RHEED patterns of samples A-D along the azimuths of the STO[100] direction.

Fig. 2. Out-of-plane θ-2θ XRD patterns of Fe_4N and samples A-D.

Fig. 3. In-plane θ-2θ XRD patterns of samples A-D around 2θ=23º.

Fig. 4. RBS depth profiles of Co, Fe, N, Au, Mg and O atoms in sample E.

Fig. 5. EDX spectra of samples A-D.

Figs. 6. (a) Out-of-plane lattice constants of samples A-D deduced from XRD peak positions plotted as a function of $\cot\theta$. (b) Corrected out-of-plane lattice constants plotted as a function of the composition ratio of $Co_xFe_{4-x}N$.

Figs. 7. (a) In-plane lattice constants of samples A-D deduced from XRD peak positions plotted as a function of $\cot\theta$. (b) Corrected in-plane lattice constants plotted as a function of the composition ratio of $Co_xFe_{4-x}N$.

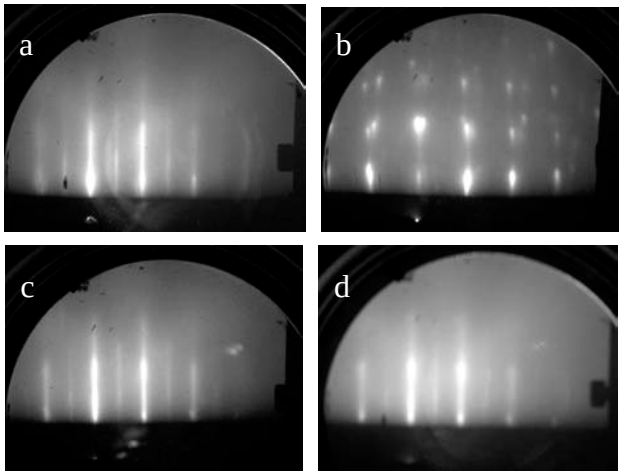

Figs. 1

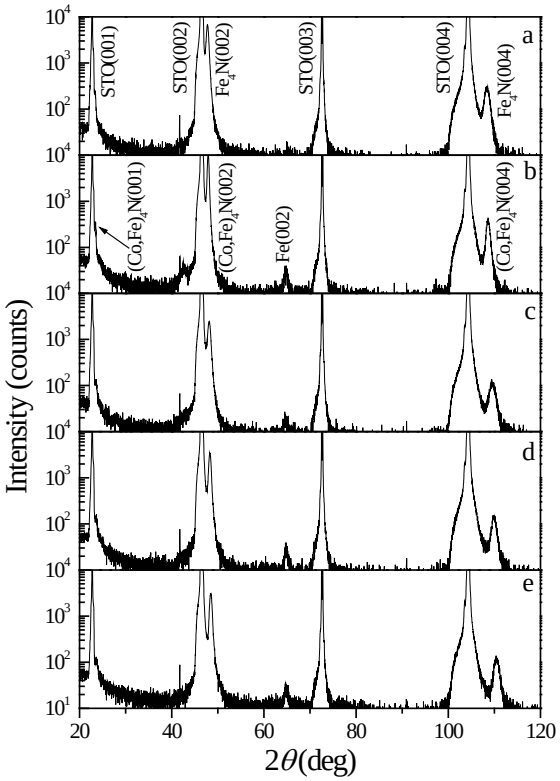
Intensity (counts)
2θ(deg)
STO(001)
STO(002)
Fe4N(002)
STO(003)
STO(004)
Fe4N(004)
(Co,Fe)4N(001)
(Co,Fe)4N(002)
Fe(002)
(Co,Fe)4N(004)
a
b
c
d
e

Fig. 2

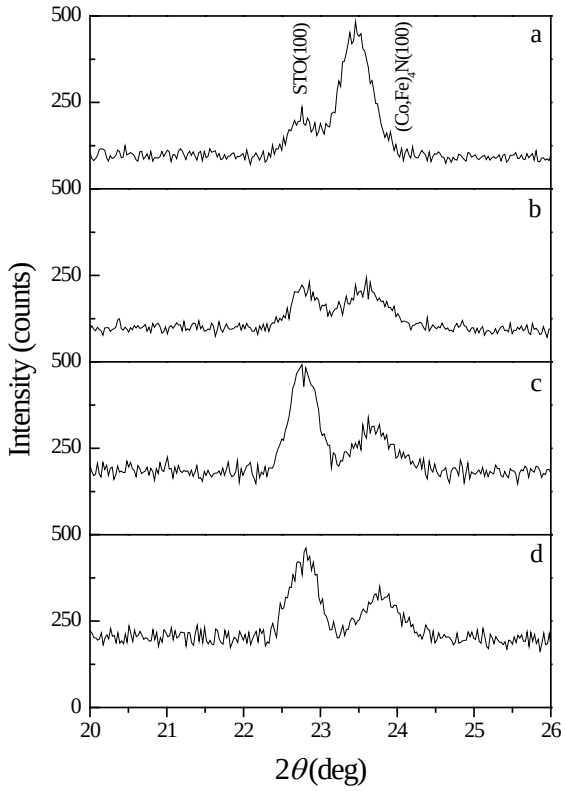
Intensity (counts)
2θ(deg)
STO(100)
(Co,Fe)4N(100)
a
b
c
d
500
250
0
20
21
22
23
24
25
26

Fig. 3

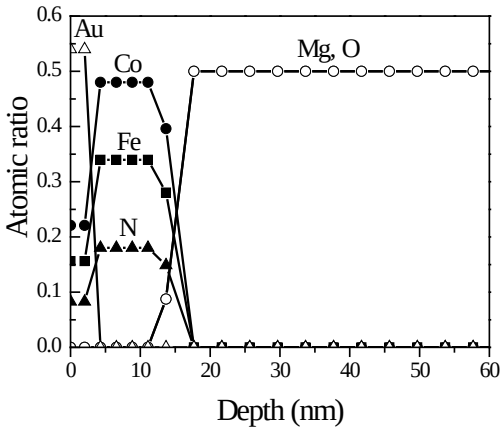
Au
Co
Mg, O
Fe
N
Atomic ratio
Depth (nm)
0.0
0.1
0.2
0.3
0.4
0.5
0.6
0
10
20
30
40
50
60

Fig. 4

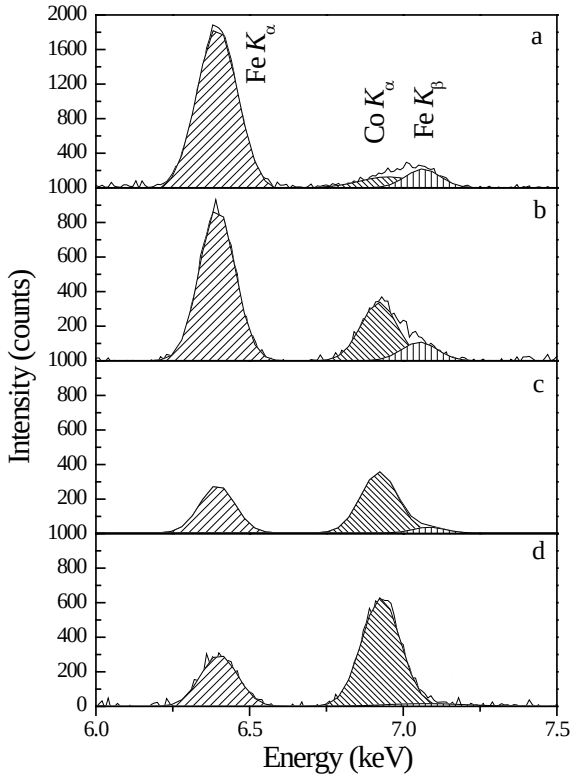
Intensity (counts)
Energy (keV)
Fe K_α
Co K_α
Fe K_β
a
b
c
d

Fig. 5

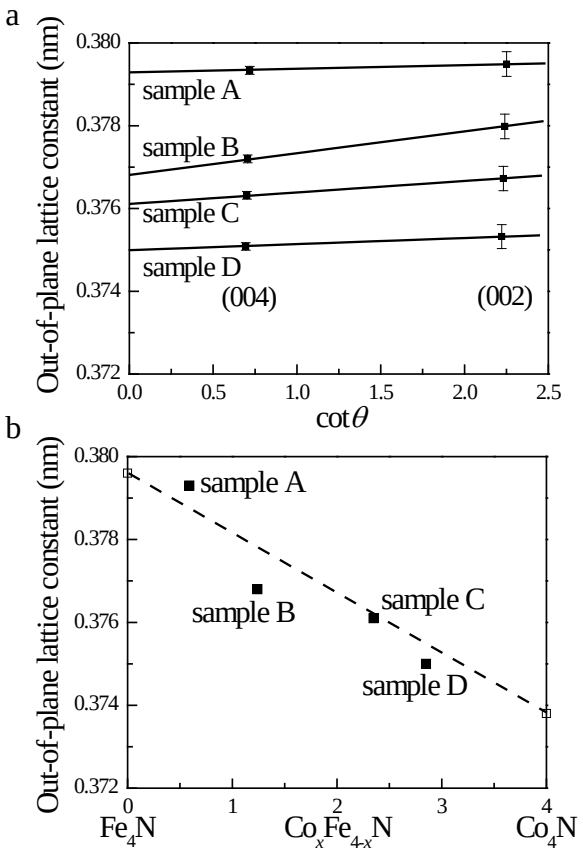
a
Out-of-plane lattice constant (nm)
0.380
0.378
0.376
0.374
0.372
sample A
sample B
sample C
sample D
(004)
(002)
0.0
0.5
1.0
1.5
2.0
2.5
cot θ
b
Out-of-plane lattice constant (nm)
0.380
0.378
0.376
0.374
0.372
sample A
sample B
sample C
sample D
0
1
2
3
4
Fe4N
CoxFe4-xN
Co4N

Figs. 6

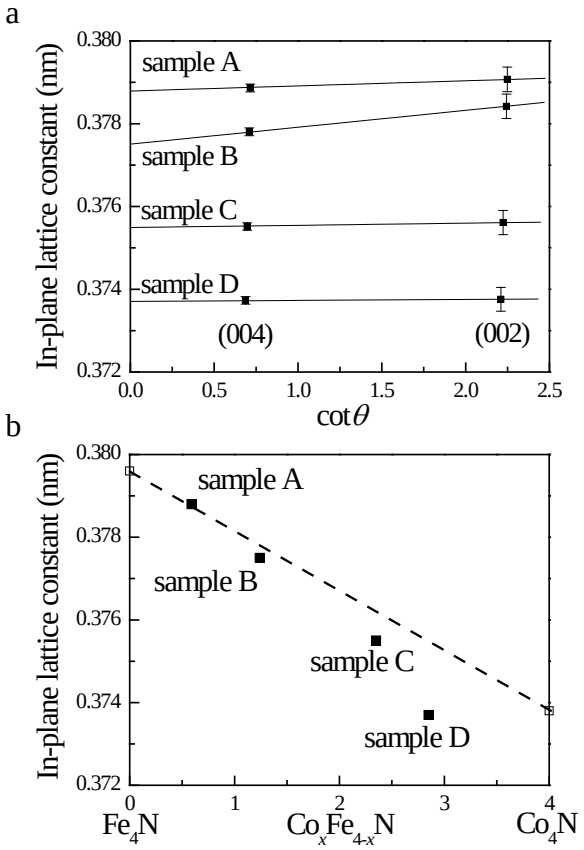
a
In-plane lattice constant (nm)
0.380
0.378
0.376
0.374
0.372
sample A
sample B
sample C
sample D
(004)
(002)
0.0
0.5
1.0
1.5
2.0
2.5
cot θ
b
In-plane lattice constant (nm)
0.380
0.378
0.376
0.374
0.372
sample A
sample B
sample C
sample D
0
1
2
3
4
Fe4N
CoxFe4-xN
Co4N

Figs. 7